Global Biogeochemical Cycles®

RESEARCH ARTICLE
10.1029/2021GB007090

Key Points:

- In a high emission scenario, oceanic CO_2 uptake is predicted to peak by 2080, then slow down and remain at about half of its peak by 2300
- The multi-century changes in uptake are expected to be dominated by changing air-sea CO_2 fluxes in the Southern and the tropical oceans
- The slowdown in uptake is caused by the decrease in CO_2 solubility and storage capacity due to changes in temperature and carbon chemistry

Supporting Information:

Supporting Information may be found in the online version of this article.

Correspondence to:

M. O. Chikamoto,
megumi.chikamoto@usu.edu

Citation:

Chikamoto, M. O., & DiNezio, P. (2021). Multi-century changes in the ocean carbon cycle controlled by the tropical oceans and the Southern Ocean. *Global Biogeochemical Cycles*, *35*, e2021GB007090. https://doi.org/10.1029/2021GB007090

Received 31 MAY 2021
Accepted 4 NOV 2021

Author Contributions:

Conceptualization: Megumi O. Chikamoto, Pedro DiNezio
Funding acquisition: Pedro DiNezio
Investigation: Megumi O. Chikamoto
Methodology: Megumi O. Chikamoto, Pedro DiNezio
Supervision: Pedro DiNezio
Validation: Megumi O. Chikamoto
Visualization: Megumi O. Chikamoto
Writing – original draft: Megumi O. Chikamoto
Writing – review & editing: Pedro DiNezio

Multi-Century Changes in the Ocean Carbon Cycle Controlled by the Tropical Oceans and the Southern Ocean

Megumi O. Chikamoto[1,2] and Pedro DiNezio[1,3]

[1]Institute for Geophysics, The University of Texas at Austin, Austin, TX, USA, [2]Now at Department of Plants, Soils and Climate, Utah State University, Logan, UT, USA, [3]Department of Atmospheric and Oceanic Sciences, University of Colorado Boulder, Boulder, CO, USA

Abstract The oceanic absorption of anthropogenic carbon dioxide (CO_2) is expected to continue in the following centuries, but the processes driving these changes remain uncertain. We studied these processes in a simulation of future changes in global climate and the carbon cycle following the RCP8.5 high emission scenario. The simulation shows increasing oceanic uptake of anthropogenic CO_2 peaking towards the year 2080 and then slowing down but remaining significant in the period up to the year 2300. These multi-century changes in uptake are dominated by changes in sea-air CO_2 fluxes in the tropical and southern oceans. In the tropics, reductions in upwelling and vertical gradients of dissolved carbon will reduce the vertical advection of carbon-rich thermocline waters, suppressing natural outgassing of CO_2. In the Southern Ocean, the upwelling of waters with relatively low dissolved carbon keeps the surface carbon relatively low, enhancing the uptake of CO_2 in the next centuries. The slowdown in CO_2 uptake in the subsequent centuries is caused by the decrease in CO_2 solubility and storage capacity in the ocean due to ocean warming and changes in carbon chemistry. A collapse of the Atlantic Meridional Overturning Circulation (AMOC) predicted for the next century causes a substantial reduction in the uptake of anthropogenic CO_2. In sum, predicting multi-century changes in the global carbon cycle depends on future changes in carbon chemistry along with changes in oceanic and atmospheric circulations in the Southern and tropical oceans, together with a potential collapse of the AMOC.

Plain Language Summary The ocean is absorbing and storing a significant fraction of anthropogenic carbon dioxide (CO_2), but we do not know if this effect will weaken in subsequent centuries with important consequences for predicting long-term climate changes. We investigated these changes in a simulation of future climate and the global carbon cycle in which atmospheric CO_2 concentrations continue to increase following a "business as usual" scenario. The simulation shows that the oceanic uptake of CO_2 will peak towards the end of this century, then slow down, but remain substantially high through the year 2300. The long-term increase in uptake is maintained by exchanges of dissolved carbon between the surface and the deep ocean in the tropical and southern oceans. The slowdown in uptake in subsequent centuries is caused by reduced solubility of CO_2 due to ocean warming and reduced ability of the ocean to absorb CO_2 due to changes in carbon chemistry. This effect is enhanced as more carbon dissolves and accumulates in the ocean. In sum, under high emissions, multi-century changes in the global carbon cycle will depend on future changes in ocean carbon chemistry as well as atmospheric and ocean changes in the tropics and the Southern Ocean.

1. Introduction

The global ocean has absorbed more than one-third of atmospheric CO_2 emitted by human activities (Ciais et al., 2013; Friedlingstein et al., 2020; Houghton, 2007; Khatiwala et al., 2009; Sabine et al., 2004; Watson et al., 2020). Modeling studies show that the ocean could increase the uptake of anthropogenic CO_2 throughout this century as atmospheric concentrations of this greenhouse gas continue to increase (Tjiputra et al., 2014; Wang et al., 2016). However, it is unclear how this uptake will evolve beyond the end of this century if atmospheric CO_2 concentrations continue to increase and eventually stabilize. Understanding these changes and its drivers is important to predict the long-term evolution of atmospheric CO_2, which also affects the prediction of how slower components of the climate system, such as the sediment system and the cryosphere, will respond

and stabilize (Archer & Brovkin, 2008; Charbit et al., 2008). Oceanic uptake of CO_2 could decline if atmospheric CO_2 concentrations continue to increase after the year 2100 (Matsumoto et al., 2010; Orr et al., 2001; Randerson et al., 2015). Multiple physical and chemical processes in the ocean could explain such a reduction in uptake efficiency. Ocean warming would decrease the solubility of CO_2 and slow down the uptake of CO_2 (Fung et al., 2005; Joos et al., 1999; Sarmiento et al., 1998; Wanninkhof & Triñanes,, 2017). Changes in ocean circulation could also reduce carbon transport and sequestration into the deep ocean (Bernardello et al., 2014). Furthermore, as anthropogenic carbon dissolves into the ocean, its ability to uptake more CO_2 is expected to decline due to the decreasing buffering capacity of the carbonate system (Riebesell et al., 2009; Sabine et al., 2004). However, the importance of multi-century changes in temperature, ocean circulation, and buffering remains largely unexplored.

Increasing atmospheric CO_2 concentrations can affect the uptake and storage of carbon by the ocean in multiple ways. First, the partial pressure of dissolved CO_2 in the ocean (pCO_2^{ocn}) will increase, but not as fast as in the partial pressure of CO_2 in the atmosphere (pCO_2^{atm}). This will increase the air-sea CO_2 exchange in regions where the ocean naturally uptakes CO_2, like the North Atlantic, and decrease the sea-air exchange in regions where the ocean naturally outgasses CO_2, such as upwelling regions in the equatorial oceans. These exchanges will be caused by an increase in pCO_2^{atm} and modulated by the processes governing the turbulent exchange of CO_2: the solubility of CO_2 in seawater, wind speed, and sea ice coverage (Wanninkhof, 1992). These processes are expected to change as the climate warms up and dissolved CO_2 accumulates in the ocean. Changes in the pCO_2 difference between the ocean and atmosphere, $\mathbf{\Delta}pCO_2 = pCO_2^{ocn} - pCO_2^{atm}$, have been found to be the main driver of predicted changes in CO_2 uptake throughout the 21st century (Sabine et al., 2013; Tjiputra et al., 2014). In the areas where $\mathbf{\Delta}pCO_2$ becomes negative due to increased atmospheric CO_2, the ocean absorbs atmospheric CO_2. Even in the areas where $\mathbf{\Delta}pCO_2$ is positive and CO_2 is naturally outgassed, decreasing $\mathbf{\Delta}pCO_2$ reduces this outgassing and contributes to a net uptake of CO_2 (Wanninkhof et al., 2013). Thus, regions where CO_2 is naturally absorbed or outgassed can play a role in the uptake and sequestration of carbon by the global ocean. Additional processes governing sea-air exchange, such as wind speed and sea ice extent, have been found to play a lesser role globally (Lovenduski et al., 2019; Tjiputra et al., 2014; Wanninkhof & Triñanes, 2017). For instance, changes in wind speed associated with shifts in the southern hemisphere westerlies as well as reductions in sea ice covered areas could enhance uptake of CO_2 over high latitudes (Bates et al., 2006; Landschützer et al., 2015; Rysgaard et al., 2011). In contrast to these regional impacts, reduced CO_2 solubility caused by anthropogenic warming could reduce uptake everywhere by rising sea surface temperatures globally (Fung et al., 2005; Joos et al., 1999; Matsumoto et al., 2010; Sarmiento et al., 1998; Wanninkhof & Triñanes, 2017).

Changes in the partial pressure of CO_2 on the ocean surface, pCO_2^{ocn}, will be governed by the rate of increase of dissolved inorganic carbon (DIC), as well as changes in alkalinity, temperature, and salinity. Long-term changes in these properties, particularly DIC and alkalinity, in turn, will be strongly influenced by changes in ocean circulation via exchanges between the surface and the deeper ocean, where these properties take longer to respond to the surface changes. As a result, upwelling regions are expected to play an important role in future changes in CO_2 uptake (Mikaloff Fletcher et al., 2006). In general, the weakening of upwelling could reduce the transport of DIC-rich deep waters to the surface, decreasing surface DIC and pCO_2^{ocn} (Tjiputra et al., 2014). However, if the ocean accumulates dissolved CO_2 on the surface, the DIC can be higher on the surface than in the deep ocean. In this case, the relatively low DIC of upwelled waters could help suppress the increase in surface DIC and pCO_2^{ocn}, promoting CO_2 uptake (Maier-Reimer & Hasselmann, 1987). These mechanisms may explain model predictions showing a four-fold increase in CO_2 uptake in the Southern Ocean by the year 2100 (Wang et al., 2016). These models also show that the equatorial Pacific could increase its net uptake by 40% by reducing outgassing by the end of this century (Wang et al., 2016). However, little is known regarding the long-term responses in these regions in subsequent centuries. The potential for the Atlantic Meridional Overturning Circulation (AMOC) slowdown may halt deep CO_2 transport and uptake in the North Atlantic for centuries (Bernardello et al., 2014; Randerson et al., 2015). In addition, the accumulation of dissolved CO_2 in the ocean is expected to change seawater carbon chemistry and make the ocean less efficient at absorbing CO_2 (Riebesell et al., 2009; Sabine et al., 2004). This efficiency is projected to decline by more than 30% in the year 2100 in the high CO_2 emission RCP8.5 scenario (Jiang et al., 2019) and could continue to decrease in subsequent centuries. Therefore, clarifying

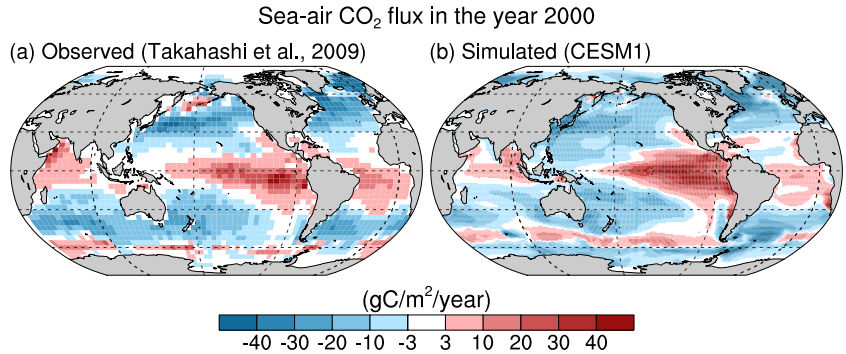

Figure 1. (a) Observed (Takahashi et al., 2009) and (b) simulated (CESM1) sea-air CO_2 flux in the year 2000. Positive (negative) flux indicates CO_2 degassing (CO_2 uptake) by the ocean.

the relative importance of these physical and chemical processes is critical to predicting long-term changes in the global carbon cycle.

Here, we quantified the influence of these processes using the output from a numerical simulation performed with the Community Earth System Model (CESM) (Moore et al., 2018), a state-of-the-art numerical model capable of simulating a highly realistic global carbon cycle (Long et al., 2013). Our goal is to assess physical and chemical processes in the ocean affecting oceanic uptake of CO_2 in subsequent centuries as atmospheric CO_2 rises and eventually stabilizes. The simulation was performed with atmospheric CO_2 concentrations following historical measurements until the year 2005 and then the RCP8.5 high emission scenario until the year 2300. According to this emission scenario, atmospheric CO_2 concentrations will peak at a value of 1,962 ppm by the year 2250 and remain stable at that level until the year 2300. This simulation allows the study of multi-century changes in oceanic uptake and outgassing of CO_2 in this century and the next two centuries. We quantified the oceanic uptake of CO_2 averaging sea-air CO_2 fluxes over key regions and estimated the influence of different processes driving changes. We also analyzed long-term trends in ΔpCO_2 and DIC to estimate the influence of changes in ocean circulation and buffering capacity of CO_2. This paper is organized as follows: Section 2 describes the CESM, the numerical simulation, and the realism of the ability of this model to simulate the global ocean carbon cycle. Section 3 presents an analysis of key regions and drivers of multi-century changes in sea-air CO_2 fluxes. The mechanisms driving long-term changes in CO_2 uptake and their impacts on the future predictions of the ocean carbon cycle are discussed in Section 4. The results and conclusions are summarized in Section 5.

2. Model and Simulation Description

We used output from a simulation of the global climate and the carbon cycle performed with the Community Earth System Model version 1.0 (CESM1) (Moore et al., 2018; Randerson et al., 2015). CESM1 simulates the interactions of the atmosphere, ocean, sea ice components, and land surface, including biogeochemical processes in the ocean and land and their exchanges of CO_2 with the atmosphere (Hurrell et al., 2013). The atmospheric component, the Community Atmosphere Model version 4 (CAM4), has a horizontal resolution of approximately $1.25° \times 0.9°$ with 26 vertical levels (Neale et al., 2013). The land component, the Community Land Model version 4 (CLM4), has the same horizontal resolution as CAM4 and has 15 vertical levels (Lawrence et al., 2012). The ocean model, the Parallel Ocean Program version 2 (POP2), has a resolution of approximately 1° and vertical 60 depth levels. In CESM1, POP2 also calculates ocean biogeochemical tracers, including DIC, alkalinity, oxygen, nutrients, and marine ecosystems (Moore & Braucher, 2008; Moore et al., 2004). These features enable the simulation of climate-carbon cycle interactions required to study changes in the ocean carbon cycle in response to increased atmospheric CO_2 concentrations and greenhouse warming.

The CESM1 simulates the spatial pattern of sea-air CO_2 flux (CO_2 flux from the ocean to the atmosphere), in good agreement with observational estimates (Figure 1). It also captures historical changes in the global average of this sea-air CO_2 flux, consistent with many observational and model-based estimates (Figure 2b). The realism

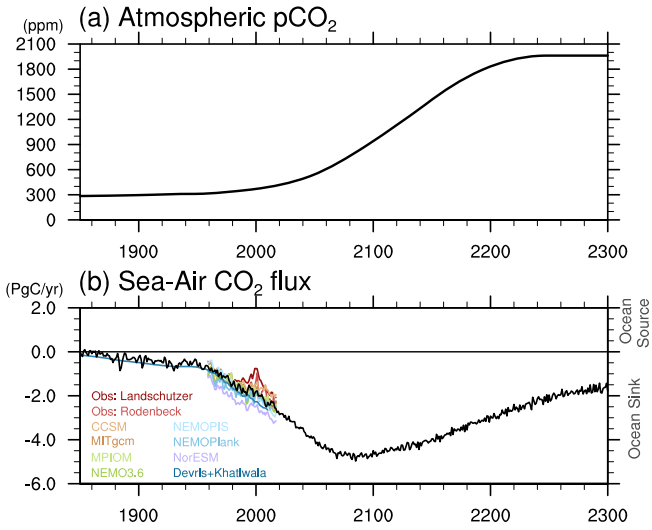

Figure 2. (a) Atmospheric CO_2 concentration (ppm) prescribed in the simulation. (b) Simulated and observed globally integrated sea-air CO_2 flux (PgC/yr). Colored lines include observational data (Landschützer et al., 2016; Rödenbeck et al., 2014), including output from eight model simulations (constrained by observations), and output from two historical simulations (all data were compiled by Le Quéré et al., 2018). Positive sea-air CO_2 flux indicates oceanic CO_2 degassing, and negative flux indicates oceanic uptake.

of the simulation allows its use to study the drivers of spatiotemporal changes in sea-air CO_2 flux. The simulation analyzed here used the CESM1, forced with historical CO_2 concentrations from the years 1850–2005 and the high emission RCP 8.5 scenario from the year 2006–2300 (Moore et al., 2018; Randerson et al., 2015). According to this scenario, atmospheric CO_2 concentrations are expected to increase rapidly in the 21st and 22nd centuries, peaking around the year 2250 at 1,962 ppm and remaining stable until the year 2300 (Figure 2a). In this simulation, oceanic CO_2 uptake and degassing do not influence atmospheric CO_2 concentrations because these concentrations are prescribed. Therefore, feedbacks between these components of the global carbon cycle are not represented. However, this type of simulation can be used to study how changes in atmospheric CO_2, ocean temperature, and ocean circulation modulate the oceanic uptake of CO_2 (Lindsay et al., 2014; Long et al., 2013). Last, the duration of this simulation allows the study of multi-century changes in the ocean carbon cycle as atmospheric CO_2 rises and stabilizes at very high levels. Few state-of-the-art earth system models have been run under the RCP8.5 scenario until the year 2300. This, together with CESM's highly realistic simulation of the ocean carbon cycle, justifies using a single model in our study.

We analyzed three intervals that characterize the main long-term changes in sea-air CO_2 flux and associated CO_2 uptake. The 2061–2100 interval captures a rapid increase in carbon uptake following the sharp rise in atmospheric CO_2 during the 21st century. A second interval from year 2141 to year 2180 captures a subsequent slowdown in the uptake of CO_2. This interval focuses on decelerating uptake, even though atmospheric CO_2 concentrations continue to increase similarly to the preceding 2061–2100 interval. The third interval spans years 2261–2300 and captures the equilibration of carbon uptake once the concentrations of CO_2 in the atmosphere stabilize. To study mechanisms driving the uptake of CO_2, we quantified the contributions to changes in sea-air CO_2 flux from changes in CO_2 solubility, wind speed, sea ice-free area, and differences in pCO_2 between the ocean and the atmosphere (Section 3.2). This analysis was performed offline using monthly variables for accounting for correlations between changes in the seasonal distributions of sea ice and wind. The calculations do not consider the higher frequency correlations between these quantities. The difference between the directly simulated sea-air CO_2 flux and the sum of the individual contributions to the flux computed offline is small. This justifies using our approach to decompose the influence of the different processes driving changes in sea-air CO_2 flux. We also quantified the influence of changes in temperature, salinity, DIC, and alkalinity in the increase in pCO_2^{ocn} (Section 3.3). These effects were estimated as tendencies driven by each quantity computed as 20-year trends using annual-mean output from the model. Using 20-year trends allowed us to capture linear changes in these quantities in order to accurately quantify their influence in the rates of pCO_2^{ocn} increase.

3. Results

3.1. Multi-Century Changes of Oceanic CO_2 Uptake

The CESM1 simulation shows the ongoing increase in oceanic uptake of CO_2 over the last 30 years in close agreement with multiple observational estimates (Figure 2b, colored lines). According to CESM1, this uptake will continue to increase through the remainder of this century, peaking around the year 2080 at 4.9 petagrams of carbon per year (PgC/yr) and then weakening and stabilizing at a level of about 1.8 PgC/yr by the year 2300 (Figure 2b). The predicted peak in oceanic uptake is consistent with the range of 3.7–5.0 PgC/yr from previous simulations also under the high emission RCP8.5 scenario (Crueger et al., 2008; Tjiputra et al., 2014; Wang et al., 2016). In our simulation, the temporal changes in the uptake of CO_2 are not spatially uniform (Figure 3). The model predicts that CO_2 uptake will intensify in the Southern Ocean from the year 2061–2300, seen as a significant negative sea-air CO_2 flux, that is, increased uptake (Figures 3b and 3c). The simulation also shows that

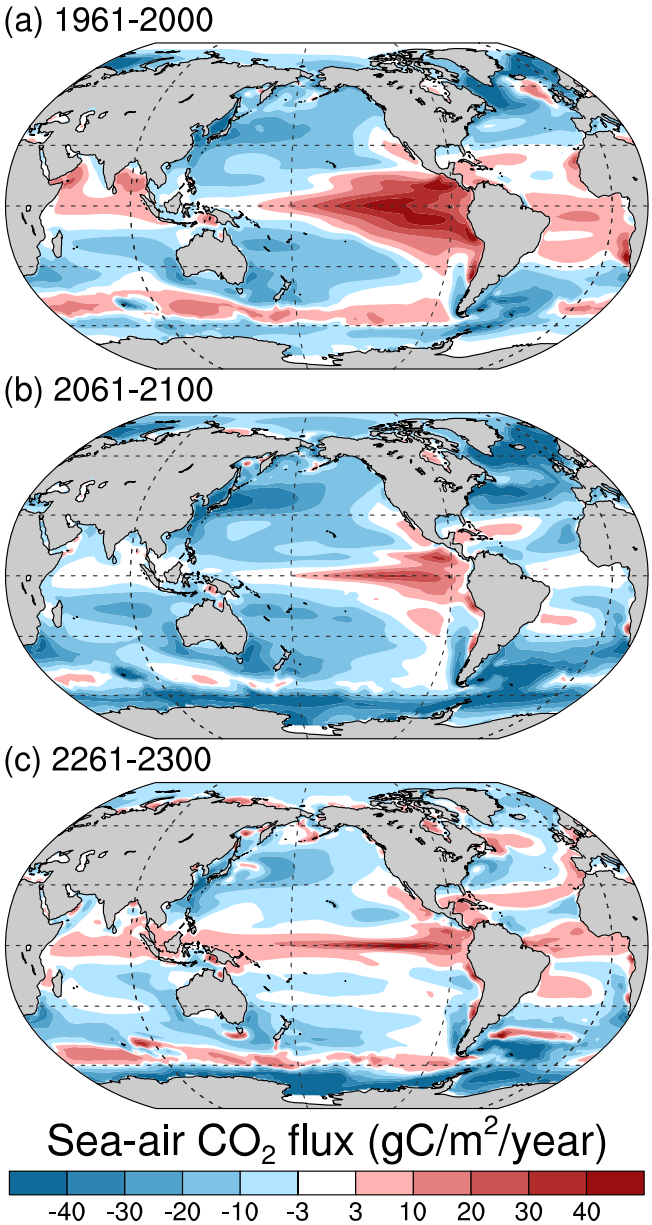

Figure 3. Annual mean sea-air CO_2 flux (gC/m^2/year) during the (a) 1961–2000, (b) 2061–2100, and (c) 2261–2300 intervals. The sea-air CO_2 flux during these intervals corresponds to (a) the ongoing uptake of anthropogenic CO_2, (b) the predicted peak towards the end of this century associated with reduced equatorial outgassing and enhanced uptake in the Southern Ocean, and (c) the nearly equilibrated final state once atmospheric CO_2 concentrations stabilize. Positive (negative) flux indicates the degassing (uptake) of CO_2 by the ocean.

the tropical oceans will continue to exhibit a positive sea-air CO_2 flux, that is, outgassing, in the period up to the year 2300, however, decreasing with time (Figures 3b and 3c). The degassing of CO_2 is predicted to change from over a large region spanning the tropical Pacific to a narrow equatorial band (Figure 3c). According to the simulation, both the Southern Ocean (south of 45°S) and the tropical oceans will be the main contributors to changes in CO_2 uptake in the global ocean (Figure 4). The North Atlantic is predicted to continue to increase CO_2 uptake until the year 2100 (Figure 3b). However, its importance is expected to diminish by the mid 22nd century (Figures 3c and 4) due to a permanent collapse of the AMOC (Figure S1 in Supporting Information S1), significantly reducing the transport of carbon-rich waters into the deep ocean. A similar reduction in uptake is simulated over the Southern Ocean between 20°S and 45°S during this period (Figure 4).

3.2. Drivers of Regional Changes in Sea-Air CO_2 Flux

The sea-air exchange of CO_2 is affected by multiple processes, the solubility of CO_2, wind speed, sea ice coverage, and the sea-air pCO_2 difference (ΔpCO_2). The equation of gas exchange flux using these factors, which is also used in CESM1, is expressed as follows (Wanninkhof, 2014; Wanninkhof et al., 2013):

$$F_{\text{est}} = k_o \times k_w \times A_{\text{noice}} \times \Delta pCO_2, \quad (1)$$

where k_o is the solubility factor, k_w is a turbulent exchange factor controlled by wind speed, and A_{noice} is the sea ice-free area. The solubility factor, k_o, is a function of sea surface temperature (SST) and sea surface salinity (SSS) (Weiss & Price, 1980). The turbulent exchange factor, k_w, depends on SST and surface wind speeds (Wanninkhof, 1992). Detailed formulations of k_o and k_w are described in the Supporting Information S1. The ice-free area, A_{noice}, ranges from 0 when the ocean is fully covered by ice to 1 when it is no ice. We estimated the sea-air CO_2 flux (F_{est}) using Equation 1 and compared it with the sea-air CO_2 flux directly computed by the model (F_{model}) to validate the accuracy of using monthly mean fields to isolate the influence of each factor. The flux estimated using Equation 1, F_{est}, accurately captures the simulated flux (F_{model}) (green and gray lines in Figure 5, respectively), confirming that Equation 1 can be used to estimate the simulated sea-air CO_2 flux, and thus isolate the influence of each factor. We only find a mismatch between $F_{\text{est}}$and F_{model} in the Southern Ocean at high latitudes (Figure 5a). This discrepancy is likely to arise from the lack of sub-monthly correlations between wind speed variability and sea ice coverage in F_{est} (Rysgaard et al., 2011). Then we estimated the influence of changes in each factor of Equation 1 to quantify the influence of the different physical processes. Our detailed methodology is available in the Supporting Information S1.

The changes in sea-air CO_2 flux are dominated by changes in ΔpCO_2 over the tropical oceans and over the 45°–55°S latitude band in the Southern Ocean (purple lines in Figures 5b and 5c). Changes in the areas covered by sea ice and wind speed drive changes in CO_2 flux over the high latitudes in the Southern Ocean (south of 55°S). These two factors contribute as much as changes in ΔpCO_2, especially after the year 2100 (Figure 5a). This means that as global warming continues, changes in sea ice coverage and wind speed will increasingly become important drivers of CO_2 uptake. Around Antarctica, a reduction in the area covered by sea ice together with a strengthen-

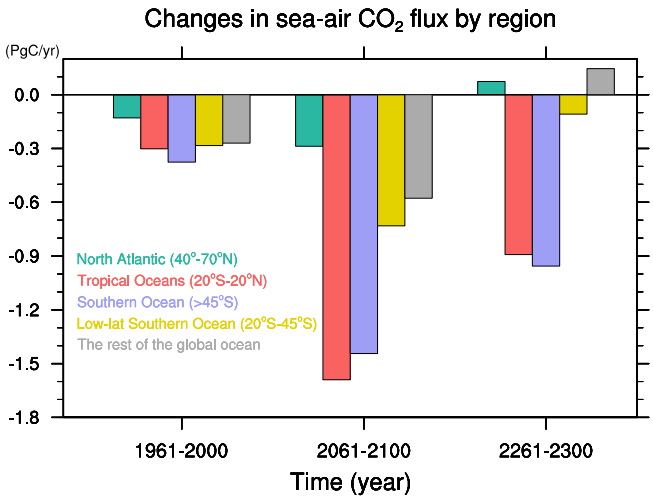

Figure 4. Region controlling changes in the oceanic CO_2 uptake. Changes in sea-air CO_2 fluxes integrated over a series of regions (PgC/yr) relative to the 1850–1889 baseline. Bars show area integrated changes over the North Atlantic (70°W–70°E, 40°N–80°N) (green), tropical oceans (0°–360°, 20°S–20°N) (red), Southern Ocean (0°–360°, >45°S) (blue), low-latitude Southern Ocean (0°–360°, 25°S–45°S) (yellow), and the rest of the world ocean (gray).

ing of westerly winds is expected to accelerate the turbulent exchange of CO_2 over the ocean (Figure 6). According to the simulation, these changes will increase the uptake of CO_2 in the period up to the year 2300 in regions where ΔpCO_2 remains negative (Figures 6c–6i). This means that as global warming continues, changes in sea ice coverage and wind speed will increasingly become important drivers of CO_2 uptake.

3.3. Drivers of Regional ΔpCO_2 Changes

Here we analyze the drivers of changes in ΔpCO_2, the main controlling factor of the multi-century changes in CO_2 uptake. Since pCO_2^{atm} is prescribed in our simulation, ΔpCO_2 is driven by changes in pCO_2^{ocn}, which is, in turn, controlled by changes in SST, SSS, surface DIC, and surface alkalinity. Alkalinity is an excess of base, which acts to weaken or buffer ocean acidity caused by CO_2 dissolution (Middelburg et al., 2020). We estimated changes in these quantities over consecutive 20-year intervals over which the simulated changes in pCO_2^{ocn} are accurately captured by linear trends (Appendix A). Our analysis focuses on key intervals at which the model predicts that pCO_2^{ocn} will increase more slowly or faster than pCO_2^{atm}, thus accelerating or slowing down the uptake of CO_2. Until the year 2100, ΔpCO_2 shows a negative trend because pCO_2^{ocn} increases more slowly than pCO_2^{atm} (blue shade in Figure 7a), and the ocean increases CO_2 uptake. Starting in the year 2100, ΔpCO_2 shows a positive trend since pCO_2^{ocn} increases faster than pCO_2^{atm} (pink shade in Figure 7a). This positive trend drives the slowdown in CO_2 uptake by the ocean, following the peak around the year 2080 (Figure 2b). This slowdown of uptake is not as large as the acceleration in the 21st century (Figure 7a). Thus, the oceanic uptake of CO_2 remains significant in the period up to the year 2300 (Figure 2b).

The changes in ΔpCO_2 are controlled by regional changes in pCO_2^{ocn} that explain the spatiotemporal differences in oceanic CO_2 uptake. In the tropical and the southern oceans, the increase in pCO_2^{ocn} is dominated by increases in surface DIC until the year 2100, with little contribution from SST and alkalinity, except over high latitudes in the Southern Ocean (Figures 7b–7d). During this period, pCO_2^{ocn} in all regions is predicted to increase at a slower rate than pCO_2^{atm}. This response indicates that surface DIC is not fully adjusted with the increasing pCO_2^{atm} during the 21st century, thus being the main control on the uptake of CO_2. From the year 2140–2180, surface warming and decreasing surface alkalinity start to play a more significant role by reducing CO_2 solubility and the ocean's capacity to store carbon. Surface pCO_2^{ocn} continues to increase during this interval in all regions, driven by increased surface DIC. Surface ocean warming and reduced alkalinity start to contribute to the increased pCO_2^{ocn} around the year 2060.

Surface ocean warming and reduced alkalinity are the main drivers of the slowdown of CO_2 uptake after the year 2100. At that time, the trends in ΔpCO_2 change sign, and CO_2 uptake begins to slow down (Figure 7a). Changes in surface DIC continue to drive increasing pCO_2^{ocn}, but at similar or lower rates than at the peak. This indicates that the processes driving changes in surface DIC continue to prevent pCO_2^{ocn} from rising as fast as pCO_2^{atm}, thus being the primary factors maintaining the uptake of CO_2 throughout the duration of the simulation. Indeed, when atmospheric CO_2 concentrations stabilize after the year 2250 (Figure 2a), increasing temperature and decreasing surface alkalinity continue to drive increasing pCO_2^{ocn}, which is offset by a negative trend driven by slowly increasing surface DIC. In addition, dissolved CO_2 accumulated in the ocean reduces the buffering capacity and the efficiency of CO_2 uptake in the ocean (Figure 8). The reduction in buffering capacity $\left(\partial\left[\mathrm{DIC}\right] / \partial\left[pCO_2^{ocn}\right]\right)$ decreases the sensitivity of DIC to changes in pCO_2^{ocn} and, in turn, increases the sensitivity of other factors such as temperature or alkalinity to changes in pCO_2^{ocn} (Riebesell et al., 2009). As a result, under high atmospheric CO_2 concentrations, surface temperature and alkalinity are more important for altering pCO_2^{ocn} and the oceanic uptake. In the simulation, the temporal changes in buffering capacity are regionally different. In the Southern Ocean, buffering capacity is predicted to decline faster than in the tropics throughout this century (Figure 8).

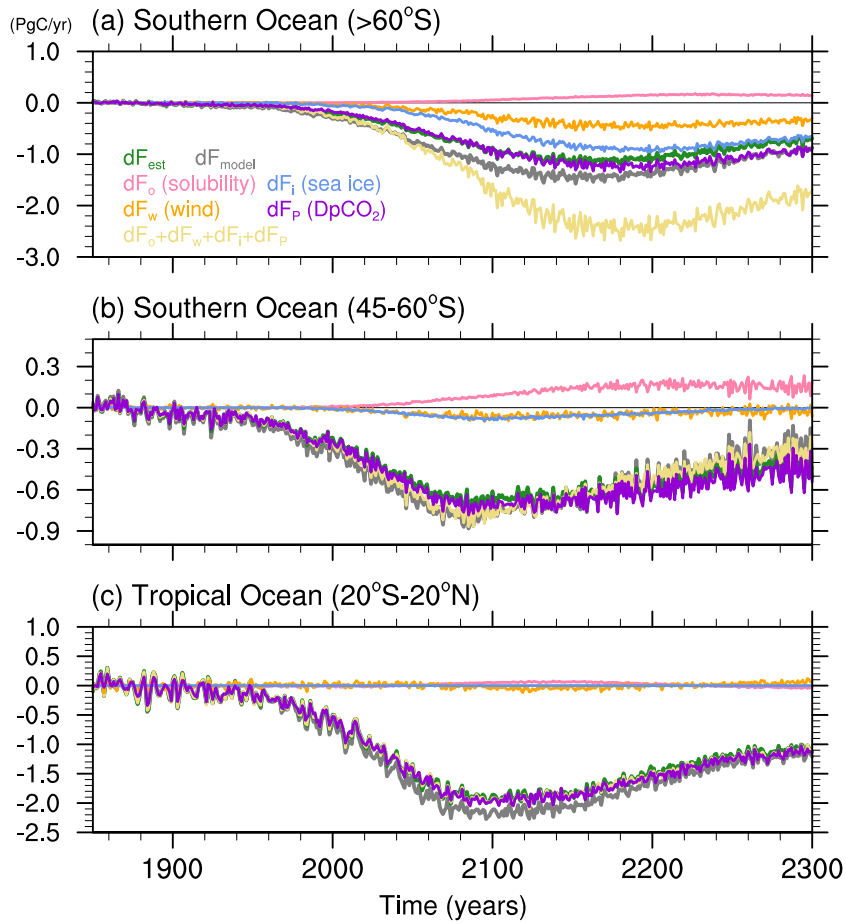

Figure 5. Influence of the solubility of CO_2, wind speeds, sea ice coverage, and ΔpCO_2 to changes in sea-air CO_2 flux. Time series of changes in sea-air CO_2 flux (PgC/yr) integrated over (a) high latitudes of the Southern Ocean (>55°S), (b) mid-latitudes of the Southern Ocean (45–55°S), and (c) the tropical oceans (20°S–20°N) relative to the 1850–1889 baseline. The colored lines show the annual average of sea-air CO_2 flux: simulated by the model (F_{model}) (gray), estimated from Equation 1 with monthly variables (F_{est}) (green), the sum of the four effects (dF_{all}) (yellow), the solubility effect (dF_o) (pink), the wind effect (dF_w) (orange), the sea ice cover effect (dF_i) (light blue), and the ΔpCO_2 effect (dF_p) (purple).

This regional difference indicates why pCO_2^{ocn} over the Southern Ocean is more sensitive to increasing surface temperature and decreasing alkalinity than the tropics (Figures 7b–7d).

Changes in surface DIC are strongly influenced by exchanges with the deep ocean via changes in ocean circulation and upwelling. Therefore, we focused our analysis on the changes in the vertical advection of DIC influencing the ocean's surface. We contrasted two intervals: the period 2061–2100, when the uptake of CO_2 increases, versus the period 2141–2180, when the uptake slows down. At high latitudes in the Southern Ocean, the simulation shows that the surface DIC trends are smaller during the 2141–2180 interval relative to the 2061–2100 interval (Figure 9a). What drives this lesser DIC trend that slows down the increase in pCO_2^{ocn}? In both intervals, the DIC decreases with depth, and this vertical gradient between the surface and the deep ocean becomes more pronounced during the 2141–2180 interval (Figure 9b). In contrast, upwelling, measured by the vertical velocity, does not change between the two intervals (Figure 9c). Therefore, in this region, changes in the vertical gradient of DIC dominate the changes in vertical advection. DIC is much lower at the intermediate depths than the surface (Figure 9b), so the upwelling of this relatively low DIC significantly reduces the vertical advection of DIC for 2141–2180. This response is seen with a strong negative peak of advection at depths of 100–200 m (Figure 9d).

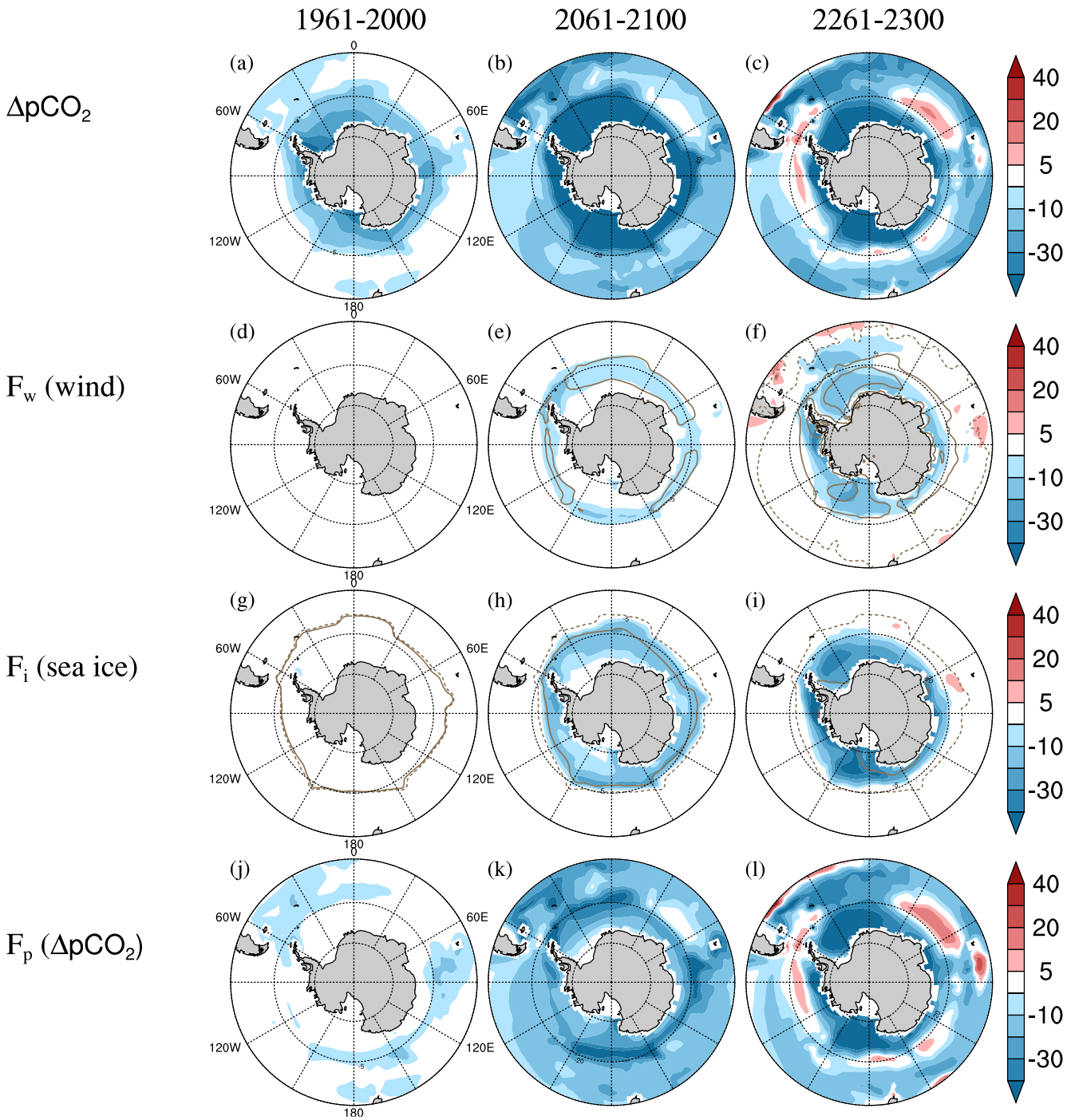

Figure 6. Drivers of sea-air CO_2 fluxes in the Southern Ocean. (a–c) The difference in pCO_2 between the ocean and atmosphere (ΔpCO_2) (ppm), and effects of (d–f) wind speed, (g–i) sea ice coverage, and (j–l) ΔpCO_2 on the sea-air CO_2 flux (gC/m^2/yr). The data are shown as differences relative to the 1850–1889 baseline. The contour lines of (d–f) are changes in surface wind speed from baseline at contour levels of ± 1 and 2 m/s (positive is solid and negative is dotted). The contour lines of (g–i) show the sea ice margin (defined by the 10%) from June to August for each period (solid) and in the 1850–1889 average (dotted).

In the tropical oceans, both upwelling changes and vertical DIC gradients are predicted to reduce vertical advection during the period 2141–2180 (Fig. 9l), slowing down the rate of increase in surface DIC. The weakening of equatorial upwelling reduces the vertical advection of DIC-rich water to the surface (Figures 9k and 9l). The vertical gradient of the DIC also weakens (Figure 9j), reducing the vertical advection with a peak near a depth of 100 m. This reduction in vertical advection slows the increase in surface DIC (Figure 9i). The slower increase in

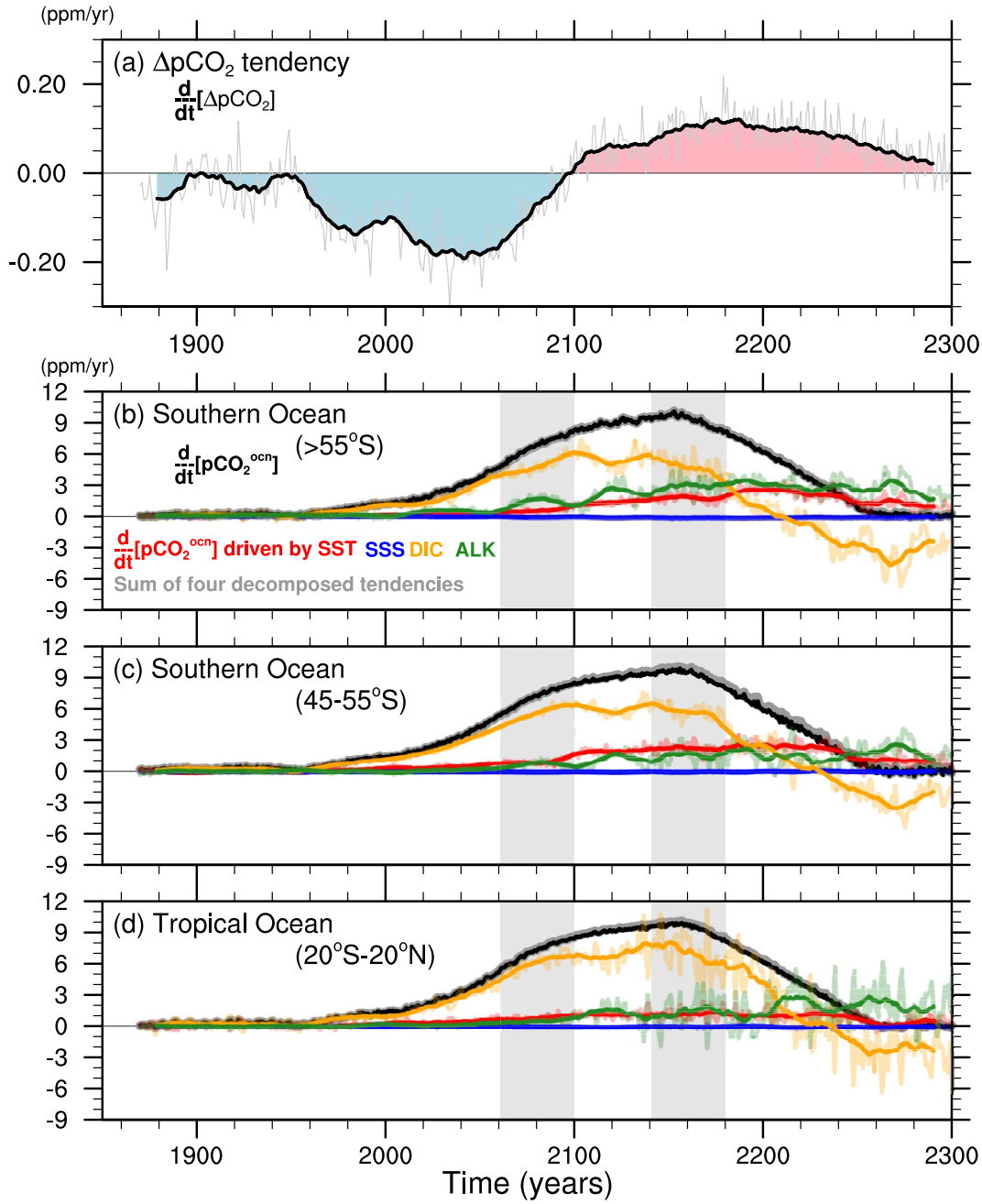

Figure 7. Drivers of pCO_2^{ocn} changes in three key regions controlling CO_2 uptake. (a) Global ΔpCO_2 tendencies, and (b–d) pCO_2^{ocn} tendencies (black line). The color lines show the tendencies in pCO_2^{ocn} driven by sea surface salinity (red), sea surface salinity (blue), surface dissolved inorganic carbon (yellow), and surface alkalinity (green). The contour lines indicate the tendencies (transparent lines) computed over consecutive 20-year intervals and these 20-year running averages (solid lines). Gray shades correspond to periods of increased and decreased net oceanic uptake.

surface DIC and pCO_2^{ocn} driven by weaker equatorial upwelling (Figure S2 in Supporting Information S1) also results in a weaker meridional gradient in surface DIC. This response reduces the advection of DIC-rich waters away from the equator. As a result, the increase in surface DIC outside the equator also slows down, preventing outgassing in a much larger area of the tropical Pacific (Figure 3c). Conversely, reduced alkalinity and enhanced warming along the equatorial Pacific drive a positive tendency on pCO_2^{ocn} and outgassing relative to the

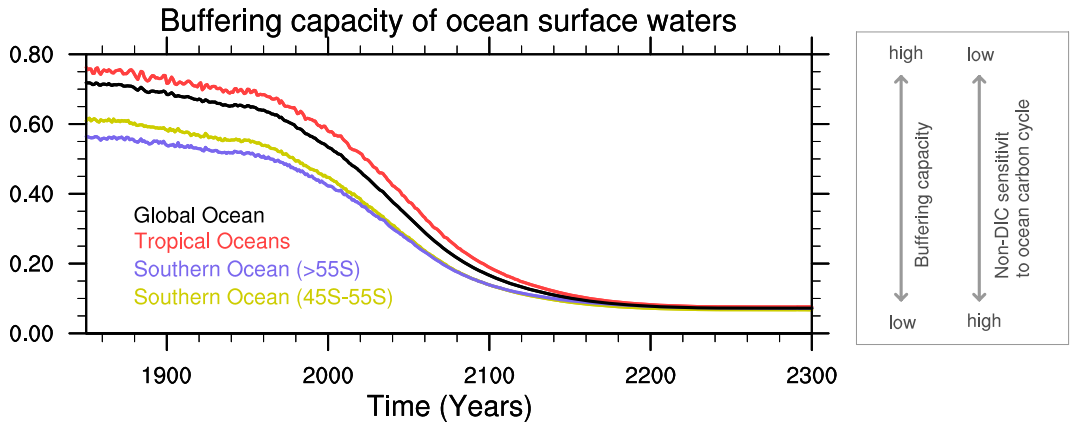

Figure 8. Changes in buffering capacity of CO_2 of ocean surface waters. Time series of regional average buffering capacity $\left(\partial\left[\mathrm{DIC}\right] / \partial\left[pCO_2^{ocn}\right]\right)$. Decreasing the buffering capacity reduces dissolved inorganic carbon (DIC) sensitivity to changes in pCO_2 and makes pCO_2 more sensitive to non-DIC factors, that is., temperature, salinity, and alkalinity.

off-equatorial regions (not shown). Combined with reduced meridional advection of DIC, these changes explain why outgassing becomes confined to the equator during this interval.

Last, uptake also increases over the mid-latitudes in the Southern Ocean (north of 55°S). According to the simulation, this region is expected to experience more downward vertical velocities at the 2141–2180 interval than at the 2061–2100 interval, indicating an increase in downwelling during this period (Figure 9g). For the 2141–2180 period, the stronger westerly winds in the Southern Hemisphere are predicted to accelerate the Deacon cell, the meridional overturning cell characterized by upwelling of deep water around Antarctica, northward transport in the Ekman layer, and sinking motion at the Antarctic convergence (Döös & Webb, 1994; Speer et al., 2000). As this circulation strengthens, its downwelling branch centered around the 45°S latitude band increases the transport of surface waters with increasingly higher DIC content into the interior ocean, slowing the increase in surface DIC (Figure 9e). This response explains the substantial reduction in the uptake of anthropogenic CO_2 at mid-latitudes in the Southern Ocean (Figure 4 with the bars).

4. Discussion

The CESM1 simulation predicts that in the high emission RCP8.5 scenario, oceanic uptake of CO_2 will peak towards the end of this century, slow down for the subsequent two centuries, but remain significant after atmospheric CO_2 concentrations stabilize. The primary process governing the temporal evolution of oceanic uptake is the negative ΔpCO_2 (sea-air pCO_2 flux) (Figure 5). This negative ΔpCO_2 during 2141–2180 is due to the slower increase in pCO_2^{ocn} than the prescribed increase in pCO_2^{atm} (Figures 7b–7d). Both changes in ocean circulation and vertical DIC distribution contribute to the long-term oceanic uptake through the reduction in ΔpCO_2. These changes are regionally heterogeneous and prominent in the upwelling and downwelling regions. In this region, changes in upwelling or weakened vertical gradients of DIC reduce vertical advection of DIC, slowing the increase of surface DIC (Figure 9). Therefore, changes in ocean circulation and vertical DIC gradient contribute to the regional response of uptake. The simulation shows that the oceanic uptake decreases from the peak of 4.9 PgC/yr around the year 2080 to 2.0 PgC/yr by the year 2300 when atmospheric CO_2 stabilizes according to the RCP8.5 scenario. The magnitude of this change is much larger than the drift of sea-air CO_2 flux in preindustrial simulations (i.e., −0.019 PgC/yr) (Lindsay et al., 2014), so the 100-year trend is less affected by the drift of the ocean carbon cycle in the model. After 2100, increasing temperature and decreasing alkalinity are predicted to accelerate the increase in pCO_2^{ocn} relative to the atmosphere, reducing their difference and uptake. In addition, the accumulation of dissolved CO_2 into the ocean decreases its buffering capacity, making pCO_2^{ocn} more sensitive to temperature and alkalinity changes than DIC (Riebesell et al., 2009). This means that temperature and alkalinity can become more important in controlling uptake as the CO_2 buffering capacity is expected to drop significantly, especially after 2100 (Figure 8). The CO_2 uptake is expected to decrease after the peak and maintain in the period

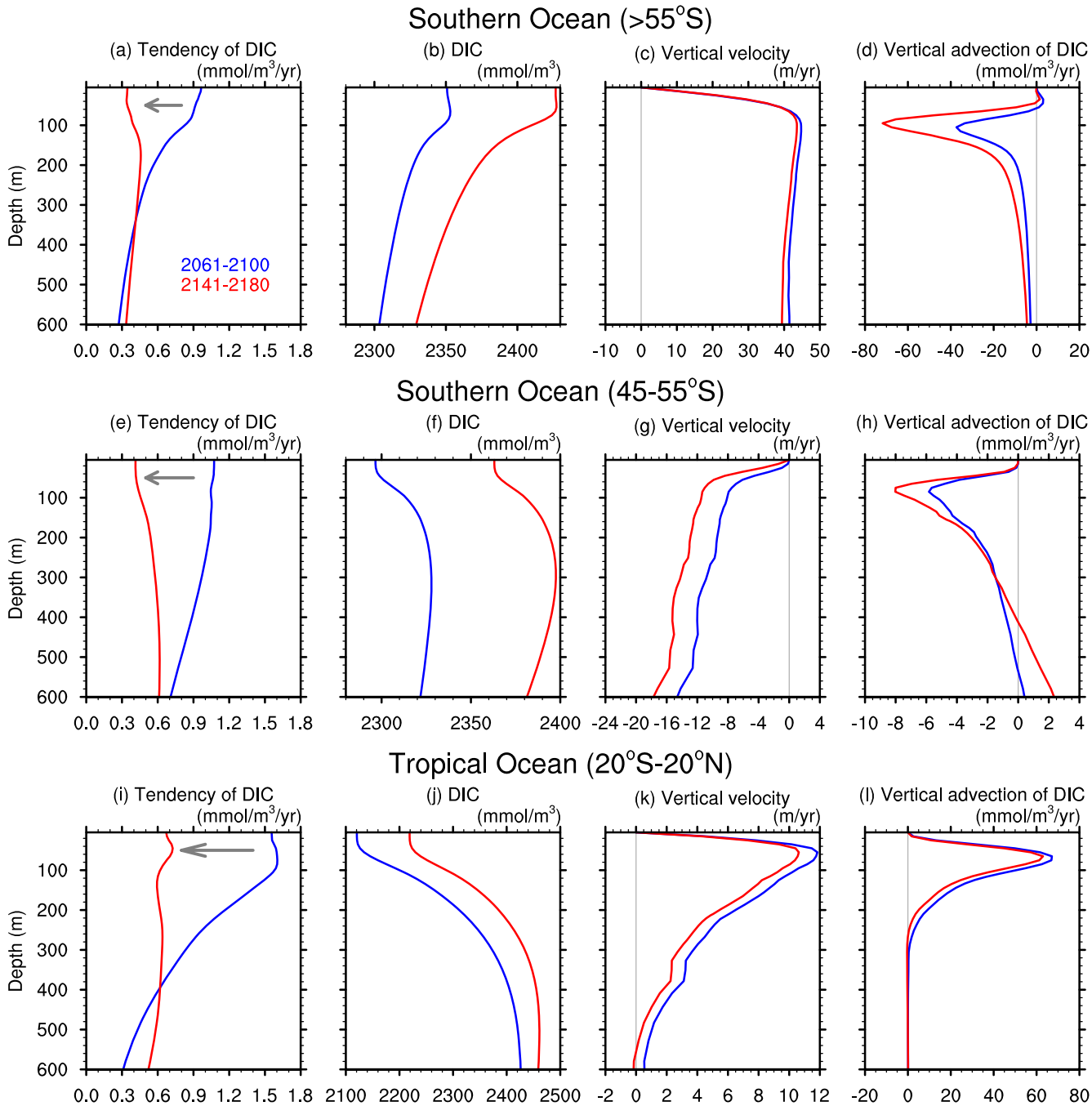

Figure 9. Trends in dissolved inorganic carbon (DIC) and vertical advection of DIC in key regions controlling CO_2 uptake. Vertical profiles of DIC tendency, DIC, vertical velocity (w; positive upward), and vertical advection of DIC. DIC is normalized by salinity. The vertical advection term was calculated as $-w\partial\left[DIC\right]/\partial z$. Colored lines indicate the key intervals when CO_2 uptake increases (blue) and slows down (red).

up to the year 2300 because surface DIC is not yet in equilibrium with atmospheric CO_2 due to changes in vertical advection and buffering capacity. This indicates that changes in DIC are not the sole driver of future changes in pCO_2^{ocn} and associated oceanic uptake, and that changes in alkalinity and temperature will also play a role in slowing uptake over the next centuries.

The changes in air-sea CO_2 flux involved in the oceanic uptake of anthropogenic carbon are predicted to be the largest in the tropical and Southern oceans. In the tropical oceans, equatorial upwelling is expected to

decrease, driven by a weakening of the equatorial trade winds in response to greenhouse warming. The associated decrease in upwelling, together with a weakened vertical gradient in dissolved carbon, will reduce the vertical advection of water with high DIC relative to those on the surface (Figures 9k and 9l). This will slow down the increase in pCO_2^{ocn} relative to the increase in pCO_2^{atm}, thus reducing the outgassing of CO_2 in this region (Figure 3). The sea-air CO_2 flux averaged over the equatorial Pacific (30°S–10°N) is predicted to decrease from 0.4 PgC/yr in 1980–2005 to −0.2 PgC/yr in 2080–2099. The magnitude of this change of 0.6 PgC/yr is consistent with the analysis of models participating in the Climate Model Intercomparison Project (CMIP5) (Wang et al., 2016). This consensus is likely due to model agreement regarding the future weakening of equatorial trade winds and upwelling (DiNezio et al., 2009; Terada et al., 2020). Therefore, accurate predictions of changes in the trade winds and tropical upwelling are critical for predicting future CO_2 uptake in the tropical oceans.

Our analysis shows that at high latitudes over the Southern Ocean, a slower increase in surface DIC and pCO_2^{ocn} relative to the increasing pCO_2^{atm} is expected to increase carbon uptake in the period up to the year 2300. Due to the higher DIC on the surface than in the intermediate depth (Figure 9b), the upwelling of relatively low DIC waters will slow down the increase in the surface DIC, thus increasing the uptake of CO_2. At mid-latitudes over the Southern Ocean, intensified downwelling, also driven by a stronger Deacon Cell in response to stronger westerly winds, is expected to increase the downward advection of surface waters (Figure 9h). This downward transport reduces the surface concentrations of DIC (Figure 9e), increasing the uptake of CO_2 over this region. Intensifying westerly winds and melting sea ice could further amplify uptake after the year 2100, as they increase the flow and area of sea-air CO_2 exchange around Antarctica. Differences in multi-model simulations of temporal changes in uptake are more pronounced in the Southern Ocean than in the tropics (Wang et al., 2016), which can be affected by changes in sea ice, upwelling, and wind speed.

Our simulation shows that the AMOC could reduce its impact on CO_2 uptake in subsequent centuries relative to this century. The AMOC strength is predicted to decrease from 31 Sverdrup (Sv) to 5 Sv by the year 2300 (Figure S1 in Supporting Information S1), consistent with other climate projections for AMOC slowdown (Collins et al., 2013; Lobelle et al., 2020; Meehl et al., 2013). Such a response will reduce the downward transport of CO_2 into the deep ocean, increasing pCO_2^{ocn} in the North Atlantic (Figure 3c). As a result, the North Atlantic will uptake very little CO_2 by the year 2300 (Figure 4). Our analysis demonstrates that future changes in the oceanic uptake of CO_2 are also sensitive to processes involving the shallow ocean circulation, playing an equally important role as the AMOC. This result supports the idea that carbon uptake can be influenced by changes in DIC occurring at mid-depths (Maier-Reimer & Hasselmann, 1987). It is also consistent with the results of sensitivity simulations in which changes in wind-driven circulation have a more significant impact on ocean carbon sequestration than an AMOC shutdown (Bernardello et al., 2014). Our study emphasizes the importance of shallow ocean circulation in the tropics, in addition to upwelling and downwelling in the Southern Ocean, to predict changes in oceanic uptake on century-long timescales.

Biological production changes have a lesser impact on the uptake of CO_2 than the abiotic processes discussed above. Today, nutrients are not fully utilized for photosynthesis in the Southern Ocean, remaining at the surface. Therefore, changes in biological production will be controlled by changes in light availability or temperature, but not by changes in nutrients, as seen in an analysis of simulations of changes in climate and marine ecosystems up to the year 2300 (Moore et al., 2018). Our analysis shows that these subtle changes in biological production will have a lesser impact on carbon uptake and sequestration into the deep ocean (Figure S2 in Supporting Information S1). In the tropical oceans, where biological production is predicted to substantially decrease due to reductions in the supply of nutrients (Moore et al., 2018), the biological impact on CO_2 uptake is offset by enhanced uptake by reducing vertical advection of DIC (Figure S2 in Supporting Information S1). The imbalance between biological production and vertical advection of DIC determines the efficiency of the amount of CO_2 transported from the surface to the deep ocean. Our finding of a lesser biological impact on oceanic uptake than changes in advection questions previous studies showing that it could play a more fundamental role in the Southern Ocean (Sarmiento et al., 1998; Yamamoto et al., 2018). The experimental approach followed by these studies isolated the response due to biotic changes assuming no changes in abiotic processes. This approach explains the heightened sensitivity of carbon uptake to biological processes relative to our analysis, where both biotic and abiotic processes are allowed to change. In addition, the sensitivity of carbon

uptake to biological change may also be model-dependent (Bopp et al., 2013). Further comparisons using multi-models and sensitivity studies help assess the effects of biological change on oceanic uptake.

Changes in biological processes can also influence the ocean uptake of CO_2 by changes in alkalinity. As the oceanic uptakes CO_2, it becomes more acidic, reducing the ocean surface saturation state with respect to calcium carbonate. This reduced saturation of this mineral diminishes the ability of many species to produce their calcium carbonate shells and skeletons (Gattuso et al., 1998). As a result, the concentration of calcium ions in the ocean increases, and with that, also does surface alkalinity (Sarmiento & Gruber, 2006; Zeebe & Wolf-Gladrow, 2001). The increased alkalinity neutralizes CO_2 dissolved in the ocean, lowering ocean pCO_2 and increasing the difference with the atmosphere, thus enhancing uptake of CO_2 (Zondervan et al., 2001). Together these processes act as a negative feedback loop that tends to enhance the uptake of CO_2, counteracting the effect of reduced alkalinity (Gattuso et al., 2015; Riebesell et al., 2009; Zhang & Cao, 2016). The CO_2-calcification feedback loop described above could be more important for stabilizing the ocean carbon cycle, however, it is not typically included in simulations like ours. Therefore, it is important to quantify the strength of this feedback and represent it in models to more accurately predict long-term changes in the ocean carbon cycle.

The simulation analyzed here considered future changes in atmospheric CO_2 based on the RCP8.5 high CO_2 emission scenario. The atmospheric CO_2 levels were prescribed to follow this scenario over time, and therefore they could not respond to changes in oceanic CO_2 uptake. Previous studies have shown that this type of simulation can predict changes in CO_2 uptake in a similar way to the more realistic simulations in which atmospheric CO_2 can respond to the changes in the ocean carbon cycle (Lehner et al., 2015). However, these studies have focused only on changes until the year 2100, which are dominated by DIC. It is unclear if all the processes revealed by our analysis are accurately represented in the calculation of atmospheric CO_2 in the RCP8.5 scenario. For instance, it has the first-order role of increasing temperature and decreasing alkalinity together with changes in equatorial upwelling in changing sea-air CO_2 exchanges. Lastly, our analysis demonstrates that under a high emission scenario, the oceanic uptake of CO_2 will persist well into the 23rd century, ultimately helping atmospheric CO_2 decrease as the global carbon cycle reaches equilibrium. This long-term ocean response is not entirely realistic due to the lack of carbon-concentration feedback from the ocean carbon cycle to the atmospheric CO_2 (Boer & Arora, 2009). It also differs from the millennial-scale CO_2 response when the coupled sediment system is included (Archer et al., 1998; Lord et al., 2016). Thus, in order to predict how atmospheric CO_2 will reach equilibrium once emissions cease, future studies should consider changes in the ocean and the sediment system occurring on centennial and millennial timescales, respectively.

5. Conclusions

We have studied the mechanisms whereby the ocean is expected to uptake CO_2 in this and subsequent centuries using a simulation of the global climate and carbon cycle performed with the CESM1. Under the high emissions RCP8.5 scenario, this simulation shows that oceanic uptake of CO_2 will peak towards the end of the 21st century, weakening thereafter while atmospheric pCO_2 continues to rise (Figure 2b). Most studies have investigated oceanic CO_2 uptake up to the year 2100 (Friedlingstein et al., 2014; Tjiputra et al., 2014; Wang et al., 2016), but this simulation shows that this uptake, and the driving mechanisms, will significantly change in the subsequent two centuries. According to the simulation, the uptake of CO_2 will be maintained by changes in shallow ocean circulation, such as reduced equatorial upwelling, slowing down the increase in surface DIC. This slow adjustment of surface DIC to rising atmospheric pCO_2 will maintain the uptake of CO_2 for the subsequent two centuries, despite reduced efficiency due to the effects of temperature and alkalinity on CO_2 solubility and storage capacity. Similarly, at high latitudes in the Southern Ocean, surface DIC is expected to increase more slowly due to the upwelling of relatively low-DIC intermediate waters, leading to increased oceanic uptake.

After the year 2100, the uptake of CO_2 will be affected by ocean warming and decreasing alkalinity. Both factors will accelerate the rate at which ocean pCO_2 increases, reducing the difference with the atmospheric pCO_2, thus slowing down the uptake of CO_2. The influences of temperature and alkalinity are expected to become more pronounced after the year 2100 when the ocean accumulates dissolved CO_2, and thus, its buffering capacity diminishes. This occurs because the reductions in buffering capacity make oceanic pCO_2 more sensitive to changes

in surface temperature and alkalinity than to the changes in surface DIC (Figure 8). Sea ice retreat and stronger southern hemisphere westerly winds are expected to increase the uptake of CO_2 by enhancing the turbulent air-sea CO_2 exchange. However, their effects are limited to the areas around Antarctica. In sum, the shallow ocean circulation favors long-term uptake, acting as a negative feedback loop, while ocean warming and alkalinity decrease present a positive feedback on the global carbon cycle after the year 2100. In our simulation, the atmospheric CO_2 levels are prescribed to follow this scenario over time, and therefore we cannot assess how the changes in oceanic uptake of CO_2 discussed here will influence atmospheric CO_2 concentrations as the global carbon cycle equilibrates. Therefore, a fully interactive global carbon cycle, which is the atmospheric, ocean, and terrestrial carbon cycle, including long responses of sediments and weathering, is needed to better understand how atmospheric CO_2 concentrations will equilibrate after anthropogenic emission ceases.

Appendix A: Isolation of Factors That Change pCO_2^{ocn}

Ocean pCO_2, pCO_2^{ocn}, is a function of SST, SSS, DIC, and alkalinity (Sarmiento & Gruber, 2006); therefore, the tendency in pCO_2^{ocn} will be controlled by the tendencies of those quantities. Their effect on the tendency in pCO_2^{ocn} was isolated as follows.

$$\frac{\partial\left[pCO_2^{ocn}\right]}{\partial t}=\frac{\partial\left[pCO_2^{ocn}\right]}{\partial T}\cdot\frac{\partial T}{\partial t}+\frac{\partial\left[pCO_2^{ocn}\right]}{\partial S}\cdot\frac{\partial S}{\partial t}+\frac{\partial\left[pCO_2^{ocn}\right]}{\partial\left[DIC\right]}\cdot\frac{\partial\left[DIC\right]}{\partial t}+\frac{\partial\left[pCO_2^{ocn}\right]}{\partial\left[ALK\right]}\cdot\frac{\partial\left[ALK\right]}{\partial t}, \quad (A1)$$

where the first, second, third, and fourth terms on the right-hand side are tendencies in pCO_2^{ocn} driven by SST, SSS, surface DIC, and surface alkalinity. Each term in Equation A1 was calculated using consecutive 20-year intervals in which the simulated changes in pCO_2^{ocn} are accurately captured by a linear trend.

The terms on the right side of Equation A1 can be further decomposed as

$$\frac{\partial\left[pCO_2^{ocn}\right]}{\partial T}\cdot\frac{\partial T}{\partial t}=\frac{\partial T}{\partial t}\times\left[pCO_2^{ocn}\right]\times\frac{\partial\ln\left[pCO_2^{ocn}\right]}{\partial T}, \quad (A2)$$

$$\frac{\partial\left[pCO_2^{ocn}\right]}{\partial S}\cdot\frac{\partial S}{\partial t}=\frac{\partial S}{\partial t}\times\frac{\left[pCO_2^{ocn}\right]}{S}\times\frac{\partial\ln\left[pCO_2^{ocn}\right]}{\partial lnS}, \quad (A3)$$

where $\partial\ln\left[pCO_2^{ocn}\right]/\partial T$ and $\partial\ln\left[pCO_2^{ocn}\right]/\partial lnS$ are the sensitivities of pCO_2 to changes in SST and SSS, 0.0423 ($^oC^{-1}$) and 1.0, respectively (Sarmiento & Gruber,, 2006).

Similarly, the DIC and alkalinity terms of Equation A1 were further decomposed. The addition of freshwater dilutes the ocean surface concentrations of properties, such as DIC and alkalinity, which affects the trend of pCO_2^{ocn}. To consider this freshwater effect on pCO_2^{ocn}, we used salinity normalized DIC and alkalinity in the following equations:

$$\frac{\partial\left[pCO_2^{ocn}\right]}{\partial\left[DIC\right]}\cdot\frac{\partial\left[DIC\right]}{\partial t}=\frac{\partial\left[pCO_2^{ocn}\right]}{\partial\left[DIC\right]}\cdot\frac{\partial}{\partial t}\left(\frac{S}{S_o}\left[sDIC\right]\right)=\frac{\partial\left[pCO_2^{ocn}\right]}{\partial\left[DIC\right]}\left(\frac{\left[sDIC\right]}{S_o}\cdot\frac{\partial S}{\partial t}+\frac{S}{S_o}\cdot\frac{\partial\left[sDIC\right]}{\partial t}\right), \quad (A4)$$

$$\frac{\partial\left[pCO_2^{ocn}\right]}{\partial\left[ALK\right]}\cdot\frac{\partial\left[ALK\right]}{\partial t}=\frac{\partial\left[pCO_2^{ocn}\right]}{\partial\left[ALK\right]}\cdot\frac{\partial}{\partial t}\left(\frac{S}{S_o}\left[sALK\right]\right)=\frac{\partial\left[pCO_2^{ocn}\right]}{\partial\left[ALK\right]}\left(\frac{\left[sALK\right]}{S_o}\cdot\frac{\partial S}{\partial t}+\frac{S}{S_o}\cdot\frac{\partial\left[sALK\right]}{\partial t}\right), \quad (A5)$$

where $\left[sDIC\right]$ and $\left[sALK\right]$ are the concentrations of salinity normalized surface DIC and alkalinity. These are expressed as $\left[sDIC\right]=S_o/S\left[DIC\right]$ and $\left[sALK\right]=S_o/S\left[ALK\right]$ and they were using the reference salinity of S_o (35 psu). The value of $\partial\left[pCO_2^{ocn}\right]/\partial\left[DIC\right]$ is the sensitivity of pCO_2^{ocn} to changes in DIC. The inverse ratio of this sensitivity, that is, $\partial\left[DIC\right]/\partial\left[pCO_2^{ocn}\right]$, indicates the CO_2 buffering capacity of ocean waters (Riebesell et al., 2009). The following steps show how to compute $\partial\left[pCO_2^{ocn}\right]/\partial\left[DIC\right]$, as shown in the previous

study (Palevsky & Quay, 2017). First, we calculated pCO_2^{ocn} from the annual average data of the model output of SST, SSS, surface DIC, and surface alkalinity. Then, we additionally calculated pCO_2^{ocn} using the same annual average data but with surface DIC plus 1 mmol/m^3. Last, the values of these pairs were subtracted. This subtraction value indicates the change in pCO_2^{ocn} with respect to the change in DIC at 1 mmol/m^3. The value of $\partial\left[pCO_2^{ocn}\right] / \partial\left[\mathrm{ALK}\right]$ was calculated in the same way as $\partial\left[pCO_2^{ocn}\right] / \partial\left[\mathrm{DIC}\right]$, but with a change in alkalinity. The global average of $\partial\left[pCO_2^{ocn}\right] / \partial\left[\mathrm{DIC}\right]$ is estimated to increase from 1.5 in the year 1850 to 13 in the year 2300, and buffering capacity will decrease from 0.72 to 0.07, down to 10% (Figure 8). The sum of the four effects is close to the pCO_2^{ocn} tendency (gray and black line in Figures 7b–7d), indicating that our approach captures the overall change in pCO_2^{ocn}.

Data Availability Statement

The series of the earth system simulation in CESM1 that we analyzed in this study were downloaded from https://www.earthsystemgrid.org/dataset/ucar.cgd.ccsm4.randerson2015.html. The observational data of sea-air CO_2 flux in Figure 1a were downloaded from https://www.ldeo.columbia.edu/res/pi/CO2/carbondioxide/pages/air_sea_flux_2010.html. Compiled data of sea-air CO_2 fluxes by the observations and model outputs of Figure 2 were obtained from https://www.icos-cp.eu/science-and-impact/global-carbon-budget/2018 (Le Quéré et al., 2018).

Acknowledgments
M.C. and P.D. were supported by NSF grant OCE-1635465.

References

Archer, D., & Brovkin, V. (2008). The millennial atmospheric lifetime of anthropogenic CO_2. *Climatic Change*, *90*, 283–297. https://doi.org/10.1007/s10584-008-9413-1

Archer, D., Kheshgi, H., & Maier-Reimer, E. (1998). Dynamics of fossil fuel CO_2 neutralization by marine $CaCO_3$. *Global Biogeochemical Cycles*, *12*, 259–276. https://doi.org/10.1029/98GB00744

Bates, N. R., Moran, S. B., Hansell, D. A., & Mathis, J. T. (2006). An increasing CO_2 sink in the Arctic Ocean due to sea-ice loss. *Geophysical Research Letters*, *33*. https://doi.org/10.1029/2006GL027028

Bernardello, R., Marinov, I., Palter, J. B., Sarmiento, J. L., Galbraith, E. D., & Slater, R. D. (2014). Response of the ocean natural carbon storage to projected twenty-first-century climate change. *Journal of Climate*, *27*, 2033–2053. https://doi.org/10.1175/JCLI-D-13-00343.1

Boer, G. J., & Arora, V. (2009). Temperature and concentration feedbacks in the carbon cycle. *Geophysical Research Letters*, *36*, L02704. https://doi.org/10.1029/2008GL036220

Bopp, L., Resplandy, L., Orr, J. C., Doney, S. C., Dunne, J. P., Gehlen, M., et al. (2013). Multiple stressors of ocean ecosystems in the 21st century: Projections with CMIP5 models. *Biogeosciences*, *10*(10), 6225–6245. https://doi.org/10.5194/bg-10-6225-2013

Charbit, S., Paillard, D., & Ramstein, G. (2008). Amount of CO_2 emissions irreversibly leading to the total melting of Greenland. *Geophysical Research Letters*, *35*, L12503. https://doi.org/10.1029/2008GL033472

Ciais, P., Chris, S., Govindasamy, B., Bopp, L., Brovkin, V., Canadell, J., et al. (2013). Carbon and other biogeochemical cycles. In T. F. Stocker, D. Qin, G.-K. Plattner, M. Tignor, S. K. Allen, J. Boschung, et al. (Eds.), *Climate change 2013: The physical science basis. Contribution of Working Group I to the Fifth assessment report of the Intergovernmental Panel on Climate Change* (pp. 465–570). Cambridge University Press.

Collins, M., Knutti, R., Arblaser, J., Dufresne, J. L., Fichefet, T., Friedlingstein, P., et al. (2013). Long-term climate change: Projections, commitments and irreversibility. In T. F. Stocker, D. Qin, G.-K. Plattner, M. Tignor, S. K. Allen, J. Boschung, et al. (Eds.), *Climate Change 2013-The Physical Science Basis. Contribution of Working Group I to the Fifth Assessment Report of the Intergovernmental Panel on Climate Change* (pp. 1029–1136). Cambridge University Press.

Crueger, T., Roeckner, E., Raddatz, T., Schnur, R., & Wetzel, P. (2008). Ocean dynamics determine the response of oceanic CO_2 uptake to climate change. *Climate Dynamics*, *31*, 151–168. https://doi.org/10.1007/s00382-007-0342-x

DiNezio, P. N., Clement, A. C., Vecchi, G. A., Soden, B. J., Kirtman, B. P., & Lee, S. K. (2009). Climate response of the equatorial Pacific to global warming. *Journal of Climate*, *22*, 4873–4892. https://doi.org/10.1175/2009JCLI2982.1

Döös, K., & Webb, D. J. (1994). The Deacon cell and the other Meridional cells of the Southern Ocean. *Journal of Physical Oceanography*, *24*, 429–442, https://doi.org/10.1175/1520-0485(1994)024<0429:TDCATO>2.0.CO;2

Friedlingstein, P., Meinshausen, M., Arora, V. K., Jones, C. D., Anav, A., Liddicoat, S. K., & Knutti, R. (2014). Uncertainties in CMIP5 climate projections due to carbon cycle feedbacks. *Journal of Climate*, *27*, 511–526. https://doi.org/10.1175/JCLI-D-12-00579.1

Friedlingstein, P., O'Sullivan, M., Jones, M. W., Andrew, R. M., Hauck, J., Olsen, A., et al. (2020). Global carbon budget 2020. *Earth System Science Data*, *12*, 3269–3340. https://doi.org/10.5194/essd-12-3269-2020

Fung, I. Y., Doney, S. C., Lindsay, K., & John, J. (2005). Evolution of carbon sinks in a changing climate. *Proceedings of the National Academy of Sciences of the United States of America*, *102*, 11201–11206. https://doi.org/10.1073/pnas.0504949102

Gattuso, J. P., Frankignoulle, M., Bourge, I., Romaine, S., & Buddemeier, R. W. (1998). Effect of calcium carbonate saturation of seawater on coral calcification. *Global and Planetary Change*, *18*, 37–46. https://doi.org/10.1016/S0921-8181(98)00035-6

Gattuso, J. P., Magnan, A., Bille, R., Cheung, W. W. L., Howes, E. L., Joods, F. P., et al. (2015). Contrasting futures for ocean and society from different anthropogenic CO_2 emissions scenarios. *Science*, *349*. https://doi.org/10.1126/science.aac4722

Houghton, R. A. (2007). Balancing the global carbon budget. *Annual Review of Earth and Planetary Sciences*, *35*, 313–347. https://doi.org/10.1146/annurev.earth.35.031306.140057

Hurrell, J. W., Holland, M. M., Gent, P. R., Ghan, S., Kay, J. E., Kushner, P. J., et al. (2013). The community earth system model: A framework for collaborative research. *Bulletin of the American Meteorological Society*, *94*, 1339–1360. https://doi.org/10.1175/BAMS-D-12-00121.1

Jiang, L. Q., Carter, B. R., Feely, R. A., Lauvset, S. K., & Olsen, A. (2019). Surface ocean pH and buffer capacity: Past, present and future. *Scientific Reports*, *9*. https://doi.org/10.1038/s41598-019-55039-4

Joos, F., Plattner, G. K., Stocker, T. F., Marchal, O., & Schmittner, A. (1999). Global warming and marine carbon cycle feedbacks on future atmospheric CO_2. *Science*, *284*, 464–467. https://doi.org/10.1126/science.284.5413.464

Khatiwala, S., Primeau, F., & Hall, T. (2009). Reconstruction of the history of anthropogenic CO_2 concentrations in the ocean. *Nature*, *462*, 346–349. https://doi.org/10.1038/nature08526

Landschützer, P., Gruber, N., & Bakker, D. C. E. (2016). Decadal variations and trends of the global ocean carbon sink. *Global Biogeochemical Cycles*, *30*, 1396–1417. https://doi.org/10.1002/2015GB005359

Landschützer, P., Gruber, N., Haumann, F. A., Rodenbeck, C., Bakker, D. C., Van Heuven, S., et al. (2015). The reinvigoration of the Southern Ocean carbon sink. *Science*, *349*, 1221–1224. https://doi.org/10.1126/science.aab2620

Lawrence, D. M., Oleson, K. W., Flanner, M. G., Fletcher, C. G., Lawrence, P. J., Levis, S., et al. (2012). The CCSM4 land simulation, 1850-2005: Assessment of surface climate and new capabilities. *Journal of Climate*, *25*, 2240–2260. https://doi.org/10.1175/JCLI-D-11-00103.1

Le Quéré, C., Andrew, R. M., Friedlingstein, P., Sitch, S., Hauck, J., Pongratz, J., et al. (2018). Global carbon budget 2017. *Earth System Science Data*, *10*, 2141–2194. https://doi.org/10.5194/essd-10-2141-2018

Lehner, F., Joos, F., Raible, C. C., Mignot, J., Born, A., Keller, K. M., & Stocker, T. F. (2015). Climate and carbon cycle dynamics in a CESM simulation from 850 to 2100 CE. *Earth Syst. Dyn.*, *6*, 411–434. https://doi.org/10.5194/esd-6-411-2015

Lindsay, K., Bonan, G. B., Doney, S. C., Hoffman, F. M., Lawrence, D. M., Long, M. C., et al. (2014). Preindustrial-control and twentieth-century carbon cycle experiments with the Earth system model CESM1(BGC). *Journal of Climate*, *27*, 8981–9005. https://doi.org/10.1175/JCLI-D-12-00565.1

Lobelle, D., Beaulieu, C., Livina, V., Sévellec, F., & Frajka-Williams, E. (2020). Detectability of an AMOC decline in current and projected climate changes. *Geophysical Research Letters*, *47*. https://doi.org/10.1029/2020GL089974

Long, M. C., Lindsay, K., Peacock, S., Moore, J. K., & Doney, S. C. (2013). Twentieth-century oceanic carbon uptake and storage in CESM1(BGC). *Journal of Climate*, *26*, 6775–6800. https://doi.org/10.1175/JCLI-D-12-00184.1

Lord, N. S., Ridgwell, A., Thorne, M. C., & Lunt, D. J. (2016). An impulse response function for the "long tail" of excess atmospheric CO_2 in an Earth system model. *Global Biogeochemical Cycles*, *30*, 2–17. https://doi.org/10.1002/2014GB005074

Lovenduski, N. S., Yeager, S. G., Lindsay, K., & Long, M. C. (2019). Predicting near-term variability in ocean carbon uptake. *Earth System Dynamics*, *10*, 45–57. https://doi.org/10.5194/esd-10-45-2019

Maier-Reimer, E., & Hasselmann, K. (1987). Transport and storage of CO_2 in the ocean-An inorganic ocean-circulation carbon cycle model. *Climate Dynamics*, *2*, 63–90. https://doi.org/10.1007/BF01054491

Matsumoto, K., Tokos, K. S., Chikamoto, M. O., & Ridgwell, A. (2010). Characterizing post-industrial changes in the ocean carbon cycle in an Earth system model. *Tellus Series B Chemical and Physical Meteorology*, *62*, 296–313. https://doi.org/10.1111/j.1600-0889.2010.00461.x

Meehl, G. A., Washington, W. M., Arblaster, J. M., Hu, A., Teng, H., Kay, J. E., et al. (2013). Climate change projections in CESM1(CAM5) compared to CCSM4. *Journal of Climate*, *26*, 6287–6308. https://doi.org/10.1175/JCLI-D-12-00572.1

Middelburg, J. J., Soetaert, K., & Hagens, M. (2020). Ocean alkalinity, buffering and biogeochemical processes. *Reviews of Geophysics*, *58*, e2019RG000681. https://doi.org/10.1029/2019RG000681

Mikaloff Fletcher, S. E., Gruber, N., Jacobson, A. R., Doney, S. C., Dutkiewicz, S., Gerber, M., et al. (2006). Inverse estimates of anthropogenic CO_2 uptake, transport, and storage by the ocean. *Global Biogeochemical Cycles*, *20*, GB2002. https://doi.org/10.1029/2005GB002530

Moore, J., Fu, W., Primeau, F., Britten, G. L., Lindsay, K., Long, M., et al. (2018). Sustained climate warming drives declining marine biological productivity. *Science*, *359*, 1139–1143. https://doi.org/10.1126/science.aao6379

Moore, J. K., & Braucher, O. (2008). Sedimentary and mineral dust sources of dissolved iron to the world ocean. *Biogeosciences*, *5*, 631–656. https://doi.org/10.5194/bg-5-631-2008

Moore, J. K., Doney, S. C., & Lindsay, K. (2004). Upper ocean ecosystem dynamics and iron cycling in a global three-dimensional model. *Global Biogeochemical Cycles*, *18*, a–n. https://doi.org/10.1029/2004GB002220

Neale, R. B., Richter, J., Park, S., Lauritzen, P. H., Vavrus, S. J., Rasch, P. J., & Zhang, M. (2013). The Mean Climate of the Community Atmosphere Model (CAM4) in forced SST and fully coupled experiments. *Journal of Climate*, *26*, 5150–5168. https://doi.org/10.1175/JCLI-D-12-00236.1

Orr, J. C., Maier-Reimer, E., Mikolajewicz, U., Monfray, P., Sarmiento, J. L., Toggweiler, J. R., et al. (2001). Estimates of anthropogenic carbon uptake from four three-dimensional global ocean models. *Global Biogeochemical Cycles*, *15*, 43–60. https://doi.org/10.1029/2000GB001273

Palevsky, H. I., & Quay, P. D. (2017). Influence of biological carbon export on ocean carbon uptake over the annual cycle across the North Pacific Ocean. *Global Biogeochemical Cycles*, *31*, 81–95. https://doi.org/10.1002/2016GB005527

Randerson, J. T., Lindsay, K., Munoz, E., Fu, W., Moore, J. K., Hoffman, F. M., et al. (2015). Multicentury changes in ocean and land contributions to the climate-carbon feedback. *Global Biogeochemical Cycles*, *29*, 744–759. https://doi.org/10.1002/2014GB005079

Riebesell, U., Rtzinger, A. K., & Oschlies, A. (2009). Sensitivities of marine carbon fluxes to ocean change. *Proceedings of the National Academy of Sciences of the United States of America*, *106*, 20602–20609. https://doi.org/10.1073/pnas.0813291106

Rödenbeck, C., Bakker, D. C. E., Metzl, N., Olsen, A., Sabine, C., Cassar, N., et al. (2014). Interannual sea–air CO_2 flux variability from an observation-driven ocean mixed-layer scheme. *Biogeosciences*, *11*, 4599–4613. https://doi.org/10.5194/bg-11-4599-2014

Rysgaard, S., Bendtsen, J., Delille, B., Dieckmann, G. S., Glud, R. N., Kennedy, H., et al. (2011). Sea ice contribution to the air-sea CO_2 exchange in the Arctic and Southern Oceans. *Tellus Series B Chemical and Physical Meteorology*, *63B*, 823–830. https://doi.org/10.1111/j.1600-0889.2011.00571.x

Sabine, C. L., Feely, R. A., Gruber, N., Key, R. M., Lee, K., Bullister, J. L., et al. (2004). The oceanic sink for anthropogenic CO_2. *Science*, *305*, 367–371. https://doi.org/10.1126/science.1097403

Sabine, C. L., Hankin, S., Koyuk, H., Bakker, D. C. E., Pfeil, B., Olsen, A., et al. (2013). Surface Ocean CO2 Atlas (SOCAT) gridded data products. *Earth System Science Data*, *5*, 145–153. https://doi.org/10.5194/essd-5-145-2013

Sarmiento, J. L., & Gruber, N. (2006). *Ocean biogeochemical dynamics* (pp. 1–503). Princeton University Press.

Sarmiento, J. L., Hughes, T. M. C., Stouffer, R. J., & Manabe, S. (1998). Simulated response of the ocean carbon cycle to anthropogenic climate warming. *Nature*, *393*, 245–249. https://doi.org/10.1038/30455

Speer, K., Rintoul, S. R., & Sloyan, B. (2000). The diabatic Deacon cell. *Journal of Physical Oceanography*, *30*, 3212–3222. https://doi.org/10.1175/1520-0485(2000)030<3212:TDDC>2.0.CO;2

Takahashi, T., Sutherland, S. C., Wanninkhof, R., Sweeney, C., Feely, R. A., Chipman, D. W., et al. (2009). Climatological mean and decadal change in surface ocean pCO_2, and net sea-air CO_2 flux over the global oceans. *Deep-Sea Research Part II: Topical Studies in Oceanography*, *56*, 554–577. https://doi.org/10.1016/j.dsr2.2008.12.009

Terada, M., Minobe, S., & Deutsch, C. (2020). Mechanisms of future changes in equatorial upwelling: CMIP5 intermodel analysis. *Journal of Climate*, *33*, 497–510. https://doi.org/10.1175/JCLI-D-19-0128.1

Tjiputra, J. F., Olsen, A., Bopp, L., Lenton, A., Pfeil, B., Roy, T., et al. (2014). Long-term surface pCO_2 trends from observations and models. *Tellus Series B Chemical and Physical Meteorology*, *66*, 23083. https://doi.org/10.3402/tellusb.v66.23083

Wang, L., Huang, J., Luo, Y., & Zhao, Z. (2016). Narrowing the spread in CMIP5 model projections of air-sea CO_2 fluxes. *Scientific Reports*, *6*. https://doi.org/10.1038/srep37548

Wanninkhof, R. (1992). Relationship between wind speed and gas exchange over the ocean. *Journal of Geophysical Research*, *97*, 7373–7382. https://doi.org/10.1029/92JC00188

Wanninkhof, R. (2014). Relationship between wind speed and gas exchange over the ocean revisited. *Limnology and Oceanography: Methods*, *12*, 351–362. https://doi.org/10.4319/lom.2014.12.351

Wanninkhof, R., Park, G. H., Takahashi, T., Sweeney, C., Feely, R., Nojiri, Y., et al. (2013). Global ocean carbon uptake: Magnitude, variability and trends. *Biogeosciences*, *10*, 1983–2000. https://doi.org/10.5194/bg-10-1983-2013

Wanninkhof, R., & Triñanes, J. (2017). The impact of changing wind speeds on gas transfer and its effect on global air-sea CO_2 fluxes. *Global Biogeochemical Cycles*, *31*, 961–974. https://doi.org/10.1002/2016GB005592

Watson, A. J., Schuster, U., Shutler, J. D., Holding, T., Ashton, I. G. C., Landschützer, P., et al. (2020). Revised estimates of ocean-atmosphere CO_2 flux are consistent with ocean carbon inventory. *Nature Communications*, *11*. https://doi.org/10.1038/s41467-020-18203-3

Weiss, R. F., & Price, B. A. (1980). Nitrous oxide solubility in water and seawater. *Marine Chemistry*, *8*, 347–359. https://doi.org/10.1016/0304-4203(80)90024-9

Yamamoto, A., Abe-Ouchi, A., & Yamanaka, Y. (2018). Long-term response of oceanic carbon uptake to global warming via physical and biological pumps. *Biogeosciences*, *15*, 4163–4180. https://doi.org/10.5194/bg-15-4163-2018

Zeebe, R. E., & Wolf-Gladrow, D. (2001). *CO_2 in seawater: Equilibrium, kinetics, isotopes*. *Elsevier Oceanography Series* (Vol. 65, pp. 1–346). Elsevier.

Zhang, H., & Cao, L. (2016). Simulated effect of calcification feedback on atmospheric CO_2 and ocean acidification. *Scientific Reports*, *6*, 1–10. https://doi.org/10.1038/srep20284

Zondervan, I., Zeebe, R. E., Rost, B., & Riebesell, U. (2001). Decreasing marine biogenic calcification: A negative feedback on rising atmospheric pCO_2. *Global Biogeochemical Cycles*, *15*, 507–516. https://doi.org/10.1029/2000GB001321